

New insights into cation-driven protein adsorption to the air-water interface through infrared reflection studies of bovine serum albumin

Authors: Abigail A. Enders[†], Jessica B. Clark[†], Scott M. Elliott[‡], Heather C. Allen[†]

[†]Department of Chemistry & Biochemistry, The Ohio State University, Columbus, Ohio 43210, United States

[‡]Computational Physics and Methods (CCS-2), Los Alamos National Laboratory, Los Alamos, New Mexico 87545, USA

Corresponding author

* Heather C. Allen, allen@chemistry.ohio-state.edu

Abstract

The chemistry and structure of the air-ocean interface modulates biogeochemical processes between the ocean and atmosphere and therefore impacts sea spray aerosol properties, cloud and ice nucleation, and therefore climate. Protein macromolecules are enriched in the sea surface microlayer and have complex adsorption properties due to the unique molecular balance of hydrophobicity and hydrophilicity. Bovine serum albumin was used as a model protein to investigate the dynamic surface behavior of proteins under several variable conditions including solution ionic strength, temperature, and the presence of a fatty acid monolayer at the air-water interface. Key vibrational modes of bovine serum albumin are examined via infrared reflectance-absorbance spectroscopy, a specular reflection method that ratios out the solution phase and highlights the aqueous surface, to determine, at a molecular level, the surface structural changes and factors affecting adsorption to the solution surface. Amide band reflection absorption intensities reveal the extent of protein adsorption under each set of conditions. Studies revealed nuanced behavior of protein adsorption strongly impacted by ocean relevant sodium concentrations, and somewhat surprising, the adsorption was minimally impacted by divalent cations. The interfacial chemistry and properties are of interest because ocean surface

biogeochemistry remains elusive and increased understanding of the surface in a controlled setting will help guide ocean and climate modeling.

Introduction

Proteins are an abundant macromolecule in the ocean¹⁻³ and are enriched within the sea surface microlayer (SSML).^{4,5} The SSML is operationally defined as the topmost 1-1,000 μm of the ocean, where the atmosphere and ocean have a multitude of transport mechanisms between each other.⁶ Proteins and peptides are transferred into the atmosphere via sea spray aerosols (SSAs) that form through wave breaking and bubble bursting at the air-ocean interface.^{5,7-10} SSAs are known to contain particles that nucleate cloud^{11,12} and ice formation.¹⁰ The chemical composition of SSAs is directly controlled by the SSML chemistry.¹³⁻¹⁷ However, the processes controlling surface adsorption of proteins are not well understood,^{5,18,19} and thus requires further investigation into how surface-active compounds in general are promoted to the air-sea interface under variable conditions, including temperature, salinity, and presence of other organic molecules including surfactants. The observations presented herein may improve climate models by providing insight into the chemical complexity of the ocean and its surface and aid in understanding the biogeochemical processes affecting the ocean surface.^{10,20-24}

Knowledge is limited about protein orientation at the air-water interface.^{8,25} Surface adsorption of proteins is a complicated phenomenon because of their tertiary structures²⁶ which are controlled, in part, by hydrophobicity and hydrophilicity.²⁷ This likely influences the organization of proteins at the air-water interface.^{26,27} The structure is also affected by the system's temperature,²⁸ which is variable across the ocean.²⁹ Furthermore, the function of a protein may impact the adsorption process. For example, bovine serum albumin (BSA) is a transport protein with well-known binding affinity for fatty acids, including stearic acid.^{30,31}

Meinders and coworkers previously reported observations and conformational information of protein surface adsorption, including studies of β -casein and egg serum ovalbumin, to the air-water interface via infrared reflection-absorbance spectroscopy (IRRAS).³²⁻³⁶ Additionally, the interaction with cations at neutral pH has been documented, but the effect they have on modulating protein surface adsorption varies in the literature.^{18,37,38} Langmuir and Waugh presented the first interfacial investigation of albumins, highlighting the irreversibility of films formed by proteins on pure water.³⁷ Jarvis and colleagues presented surface pressure-area (Π -A) isotherms of BSA and upon comparison to ocean slick samples, their behaviors were strikingly similar, producing analogous isotherms.³⁸ More recently, Li and coworkers presented evidence that BSA populates the surface in saline solutions more readily than in pure water.¹⁸ The unknown propensity for BSA to adsorb at the air-water interface is motivation to probe more deeply the temperature, salinity, and monolayer effects and relationships to the interfacial structure.

The structure of bovine serum albumin at the air-water interface was studied through dilational surface rheology by Noskov and colleagues in 2010.³⁹ They found that the protein underwent a conformational change at the surface where the protein unfolded and elongated along the x-axis, until surface pressures of about 12 mN/m when it began to “loop” into the water. Further work by Yuan and coworkers expanded on understanding the surface behavior of BSA by determining surface excess at variable concentrations of protein and sodium chloride salt.⁴⁰ The observed “salting up” and “salting down” effects were a function of protein concentration; low and high concentrations have salting up effects and mid-range concentrations salt down. Ulaganathan and colleagues found that β -lactoglobulin was more readily promoted to the surface in ionic solutions, but that the effect diminished at higher concentrations (mM scale).⁴¹ These results indicate that there is at first a stabilizing effect that promotes proteins to the air-water interface in ionic solutions and the effect is not linear with ionic strength. The well-studied Hofmeister effect is further evidence of the salting out

and salting in effects on proteins.⁴²⁻⁴⁶ Generally, anions have a greater effect than cations, yet the mechanism is still not fully understood. Current works hypothesized the disordering of water structure by the ions is the cause for the observed effect.⁴⁷

BSA surface adsorption at the air-water interface is also affected by surfactants. Noskov and Mikhailovskaya reported on the reduced globule charge density of BSA when sodium dodecyl sulfate (SDS) monolayers were formed at the interface.⁴⁸ At very low surfactant concentrations, the surface adsorption of BSA was observed to decrease and the surface tension was more representative of expected values for SDS monolayers. Further surfactant work by Pedraz and colleagues characterized a two-step mechanism in which Langmuir biofilms were formed with arachidic acid and BSA.⁴⁹ The process ultimately resulted in co-adsorption, where BSA interacted with the surfactant head groups in the solution phase rather than assembly at the interface.

We present an investigation into the dynamic air-aqueous interfacial adsorption process that occurs when BSA is introduced into an aqueous system. To our knowledge, this is the first study that evaluates the impact on adsorption as a function of amide peak intensity with varying solution ionic strength, temperature, and surface structure. We examine the surface structure and its changes through IRRAS measurements, which enables surface-sensitive characterization of the interfacial chemical composition. Our approach builds from the simplest system of BSA injected into pure water at 20°C and we compare the observed changes relative to this system. We connect to oceanic and atmospheric relevant conditions using an artificial sea water (ASW) solution and variable ocean surface temperatures to understand how protein adsorption is altered.

Methods

Materials and Sample Preparation

Aqueous solutions were made using ultrapure water (MilliQ Advantage A10, resistivity 18.2 MΩ). All materials were used as received except for sodium chloride (Fisher Chemical, ≥ 99%,

certified ACS) which was baked at 600°C for at least 10 hours to remove residual impurities and used to make 0.45 M NaCl in water.⁵⁰ About 35.5 g of Instant Ocean (Instant Ocean ion concentrations from manufacturer reported in the SI) salt was used to make 1 L solutions of artificial sea water (ASW) based on label recommendations. A 1 mM BSA (Sigma Aldrich, \geq 98%, heat shock fraction, pH 7) solution in water was prepared for injection. BSA solutions of concentrations 1, 50, 100, 250, 500, and 750 μ M were also prepared for analysis via ATR-FTIR and IRRAS. Stearic acid (Sigma Aldrich, \geq 98.5%, capillary GC) was dissolved in chloroform (ACROS Organics, \geq 99.8%, ACS Reagent) to make a 3 mM solution for spreading. Solutions were prepared the day before measurements, stored in a glass Pyrex container, and equilibrated to lab conditions overnight.

Infrared Spectroscopy

A PerkinElmer micro-ATR assembly was used to obtain bulk measurements of the BSA solutions to confirm amide peak assignment. Infrared Reflection-Absorbance Spectroscopy (IRRAS) spectra were collected with a modified PerkinElmer Frontier FT-IR Spectrometer using a custom, lab-built reflection system with two gold mirrors. Infrared light from the spectrometer source is incident on the first gold mirror which is angled such that the light is directed toward the sample surface at 48° relative to surface normal. The light reflected off the sample surface is collected using a second gold mirror and returned to the liquid-nitrogen cooled HgCdTe (MCT) detector. Surface-sensitive spectra are obtained by calculating reflectance-absorbance (RA) which is given as $RA = -\log(R_M/R_O)$, where R_M is the reflectivity of the sample surface and R_O is the reflectivity of the reference (background) surface. Measurements were taken using unpolarized light in the single-beam mode and averaged over 400 scans at a resolution of 4 cm^{-1} . IR response was recorded from 4000-450 cm^{-1} at every 0.5 cm^{-1} . Samples were collected using a KSV NIMA Langmuir trough (\sim 135 mL total volume) equipped with a surface tensiometer.

Solutions at 20°C were added to the trough and equilibrated for 10 minutes prior to acquiring a background measurement. In lower temperature studies, a ThermoFisher Recirculating Chiller was used with a 60:40 water and ethylene glycol solution. The equilibration time was increased to 30 minutes to ensure complete cooling. For trials with fatty acid monolayers, 18 μ L of 3 mM stearic acid in chloroform was spread dropwise onto the surface using a Hamilton gas-tight syringe and 10 minutes were allowed for solvent evaporation prior to measurement. To all solutions, 50 μ L of 1 mM bovine serum albumin in MilliQ H₂O was injected, which resulted in a final concentration of 0.37 μ M. Measurements were taken immediately after injection. All data was taken in triplicate. Spectra presented were analyzed using custom Python codes, which included conversion from single beam to reflectance-absorbance, linear background subtraction, and averaging. Experiments performed are summarized in Table 1. The concentration dependence of BSA surface adsorption was evaluated via IRRAS measurements after injection of a series of BSA concentrations at 20°C in H₂O (SI). The calculated value corresponds with the weight percent that has stable surface pressure observed in work by Graham and Phillips in 1979.

Table 1. Three different ionic strengths were used to evaluate the adsorption of BSA to the surface with and without a competing stearic acid monolayer at both 10 and 20°C. Experiments outlined here are for IRRAS measurements.

MilliQ H ₂ O				0.45 M NaCl				Instant Ocean			
No Stearic Acid		Stearic Acid		No Stearic Acid		Stearic Acid		No Stearic Acid		Stearic Acid	
10°C	20°C	10°C	20°C	10°C	20°C	10°C	20°C	10°C	20°C	10°C	20°C

Results and Discussion

We examine protein adsorption to the surface as a function of temperature, ionic strength, and surface structure (preexisting monolayer). The amount of BSA adsorbed to the aqueous surface corresponds to the intensity of the reflectance-absorbance response. Our results indicate that BSA is surface active under all conditions, however the structure of the surface and amount that adsorbs is

variable as conditions of the system are modified. Briefly, we evaluate temperature change in the system to understand the thermodynamic dependence of protein adsorption. In addition, we determine if ionic strength or presence of a monolayer enables co-adsorption to the surface.

We first evaluated solution-phase measurements of BSA to confirm amide peaks for assignment (Figure 1). Amide I is assigned to 1660 cm^{-1} and amide II to 1540 cm^{-1} .^{51,51,52} We also note that the integrated absorbance is linear with increasing concentration and provide details regarding the nature of ATR as a bulk phase measurement with variable path length (SI). Additionally, we ensure the ions in each solution do not significantly affect the O-H stretching or bending modes (SI).

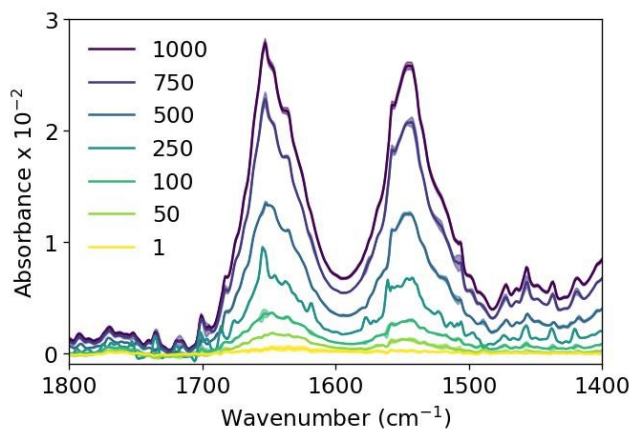


Figure 1. FTIR of BSA in water at increasing concentrations measuring solution-phase concentrations starting from $1\text{ }\mu\text{M}$ to $1000\text{ }\mu\text{M}$ shown in the amide region, presented with error of one standard deviation. The value of the standard deviation is so small it is approximately the thickness of the line of each spectrum.

Solution Effect

The solution effect on surface adsorption is observed at 20°C (Figure 2a). Surface adsorption is observed when BSA is injected into all three systems, however the intensity varies as a function of ionic composition. At ocean relevant sodium chloride concentration (0.45 M), adsorption is increased resulting in more intense negative bands (1660 cm^{-1} and 1540 cm^{-1}). The addition of divalent cations

in ASW results in a relatively small increase in intensity as compared to the NaCl solution, indicating that monovalent cations largely influence the adsorption process. ASW solution has even less of an effect on the amide II N-H bending at 1540 cm^{-1} ($\delta_{\text{N-H}}$). We observe the intensity of the amide I band increases with increasing ionic composition ($\text{H}_2\text{O} < \text{NaCl} < \text{ASW}$), which is consistent with observations described in the literature.^{40,41}

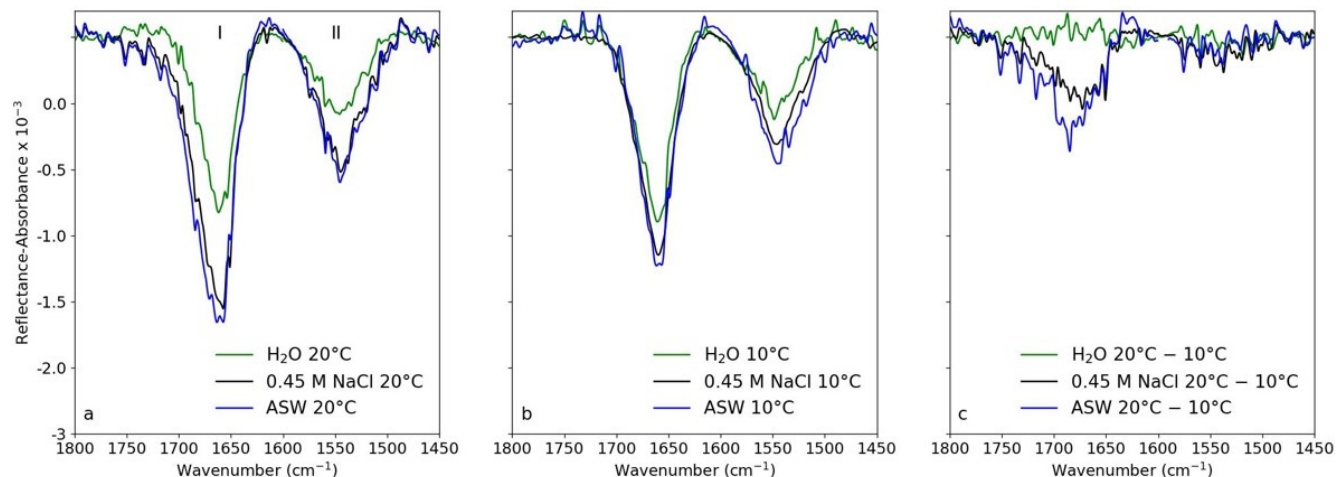


Figure 2a-c. Surface-IR responses in amide region ($1800\text{--}1450\text{ cm}^{-1}$) after bovine serum albumin (BSA) injection into the H_2O , 0.45 M NaCl , and artificial seawater solutions at **a)** 20°C , **b)** 10°C , **c)** difference spectra of $20^\circ\text{C} - 10^\circ\text{C}$. Here, reflectance-absorbance bands are observed as negative peaks.

Temperature Effect

A decrease in the solution temperature resulted in decreased peak intensity in both amide bands (Figure 2c). We observe a slightly less intense amide I band at 1660 cm^{-1} from carbonyl stretching ($\nu_{\text{C=O}}$) at 20°C for BSA in pure water. This slight change could be attributed to strengthening of H_2O -BSA hydrogen bonds as the temperature is decreased.⁵² Between 20°C and 10°C for the water solution, the amide I and II peak intensities have only a $\sim 1\%$ difference. As shown in Figure 2c, the temperature effect on surface adsorption in pure water is minimal yet has a greater impact on ionic solutions. We observe a decrease in the 1660 cm^{-1} $\nu_{\text{C=O}}$ peak intensity at 10°C

compared to 20°C for both 0.45 M NaCl and ASW. The percent difference between peak intensities at 20°C and 10°C for both 0.45 M NaCl and ASW are -5.5% and -5%, respectively.

Compared with ultrapure water at 20°C, a solution with sodium chloride greatly increases the intensity of amide I and II bands (Figure 2a). Similar trends of increased intensity in ionic solutions are observed at 10°C, but the overall intensity is decreased (Figure 2b), demonstrating that the cation stabilization of BSA at the interface is disrupted by the removal of thermal energy from the system. Our observation indicates that the addition of monovalent cations increases the propensity for protein surface adsorption in direct alignment with the “salting-out” effect that is described by the Hofmeister series.^{18,43,44} However, the ionic interactions and surface stabilization process is disrupted at decreased temperatures. The effect of the solutions is further emphasized in Figure 3, where the area under the curve is analyzed for both amide bands. We assume constant transition moment dipole strength based on our ATR analysis; the observed intensity corresponds to surface adsorption as a result.

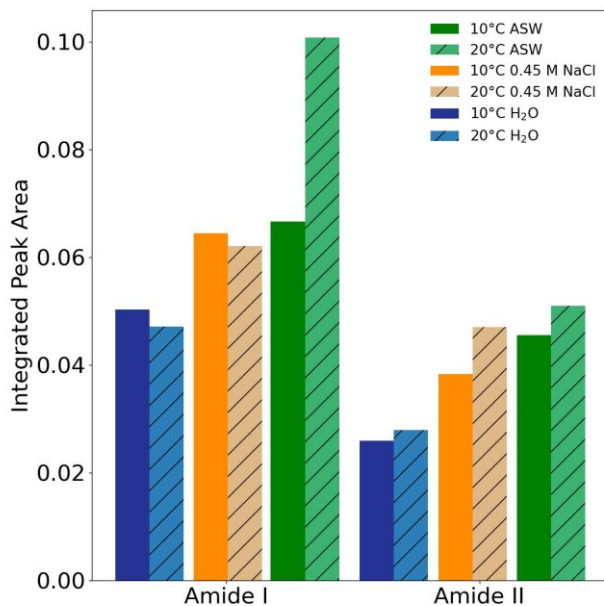


Figure 3. Integrated peak area for surface amide-I (1660 cm^{-1}) and amide-II (1540 cm^{-1}) bands at 10°C (dark blue) and 20°C (light blue). As noted, the peak area and intensity is a result of surface adsorbed protein as confirmed through bulk measurements.

BSA is negatively charged under neutral and alkaline conditions and appears to be stabilized at the surface by the sodium cations, in 0.45 M NaCl solution, at neutral pH.^{18,40,41} Increased intensity in the amide bands is attributed to the ionic strength of the solution. At 10°C, the increase in peak area is consistent with increasing ionic strength; from NaCl to ASW, the increase is relatively small. However, at 20°C, the increase is much larger between the two salt solutions. Also of note is the relatively equal peak area observed between the two temperatures in the sodium chloride solution. In the difference spectra we observe an amide I band consistent with a change in the adsorption at varying temperatures (Figure 2c). From previous literature studies, we assert this observation is occurring as a result of changing protein structure, leading to a change in the observed intensity.⁵³ We conclude that the surface adsorption of BSA is affected by both temperature and ionic interactions.

Monolayer Effect

The presence of a stearic acid monolayer ($\sim 45 \text{ \AA}^2/\text{molecule}$, gaseous phase) changes the surface adsorption of BSA at 20°C compared to the system with no monolayer at the same temperature (Figure 4a). The surface-IR spectra of the BSA/water system at the air-water interface with and without a surface adsorbed monolayer show minimal changes in peak intensity and shape. We do observe a red-shift in the $\nu_{\text{C=O}}$ of 2.5 cm^{-1} and a 5 cm^{-1} red-shift in the $\delta_{\text{N-H}}$ mode, indicating a more organized surface structure when there is a monolayer present, consistent with previous results presented in the literature.^{36,54} The effect is reversed in a 0.45 M NaCl solution at 20°C and we observe a blue-shift in each peak, indicating the surface becomes more disordered. This is likely from cationic stabilization of stearic acid and BSA. For example, cations will stabilize stearic acid at the interface through ion-dipole interactions that include ionic bonds, bridging, and chelation.⁵⁵⁻⁵⁸ We note a 7% difference between ASW with and without a fatty acid monolayer, where the lipid monolayer results in less intense amide bands.

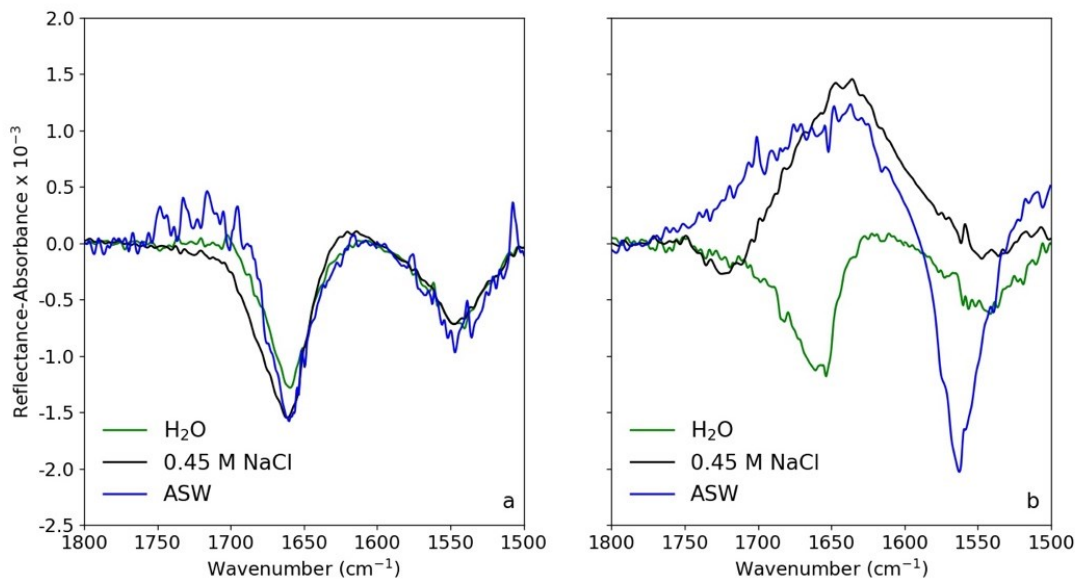


Figure 4a-b. IR response in amide region ($1800\text{-}1500\text{ cm}^{-1}$) after bovine serum albumin (BSA) injection into each solution with a stearic acid monolayer ($\sim 45\text{ \AA}^2/\text{molecule}$) on the surface at **a**) 20°C and **b**) 10°C .

The surface structure and IRRAS response becomes more complicated when the system is cooled to 10°C and a monolayer is spread. We observe similar $\nu_{\text{C=O}}$ and $\delta_{\text{N-H}}$ modes in water with similar intensities to 20°C with and without a monolayer. The 0.45 M NaCl solution has a much less intense $\delta_{\text{N-H}}$ mode and positive carbonyl stretch, which indicates that the protein is below the surface.⁵⁹ We also observe a stronger response in the ASW solution compared to 0.45 M NaCl at 10°C ; the $\nu_{\text{C=O}}$ mode is positive and $\delta_{\text{N-H}}$ is more intense. It has been previously discussed in the literature that the positive and negative peaks originate from the mathematical conversion from single beam data to reflectance-absorbance spectra due to the background subtraction.⁵⁹ Therefore, positive peaks are indicative of sub-surface IR responses. The observed derivative-like peak shape has been presented previously in the literature and attributed to the protein surface adsorption process.^{32,54,60}

We assert that the BSA must orient differently at the surface when conditions are varied based on our experimental results that are supported by literature.^{25,35,61,62} The changes that occur are not

simple or independent of other system variables. Ionic strength, temperature, and lipid monolayers have compounding effects on the observed IR response. The least complex system is ultrapure water; amide I band intensity varies only slightly when temperature and monolayers are considered. Red shifting is observed, as noted, when the stearic acid monolayer is spread and when the temperature is reduced to 10°C. Thermal energy reduction of the system results in this observed wavenumber shift, which is visualized in Figure 5. While only a small change, observing the thermodynamic effect in water indicates that the temperature does alter the system and affects how the surface adsorption and organization occurs.

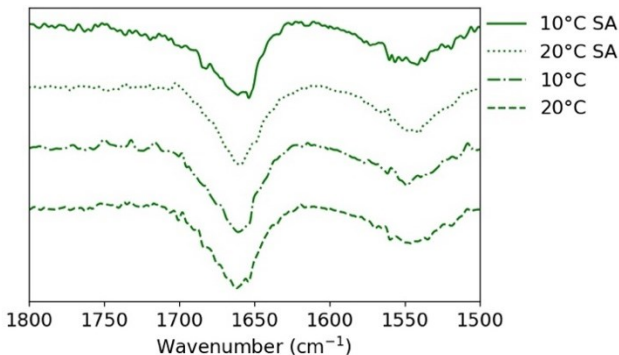


Figure 5. Spectra of ultrapure water surface after injection of bovine serum albumin (BSA) at variable temperature with and without stearic acid monolayer to emphasize the minimal intensity change in the water system. Spectra are offset horizontally for clarity.

The observed results are summarized in Figure 6. Overall, we observe smaller negative intensities on the water and have more IR response in ionic solutions (more negative RA). The temperature dependence is evident when comparing 20°C and 10°C; decreasing temperature decreases the amount of BSA adsorbing to the surface. Our results indicate that temperature effects the surface structure: decreasing the system's temperature decreases the adsorption to the surface as reflected in the lower IR response. We assert that variable temperatures over the ocean surface must influence adsorption to the air-ocean interface and the effect should be considered in climate models.

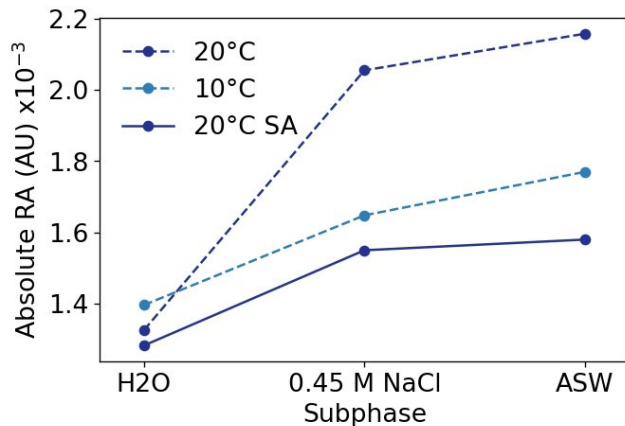


Figure 6. Observed maximum intensity of amide I band (1660 cm^{-1}) for each solution at varying temperatures. IR responses from each solution with stearic acid monolayer at 10°C are not included due to the variability in the amide I and II region.

Conclusions

Herein, we have presented evidence supporting the surface activity and adsorption process of BSA to the interface under varying ionic strength and surface conditions. The amount of adsorbed BSA is dependent on the interfacial chemistry and solution ionic strength at the time it is injected into the system. We determine that even in pure water, BSA is surface active. However, ions promote more BSA to the surface, consistent with observations previously presented in the literature.^{18,31} However, divalent cations have little effect at ocean relevant concentrations. We conclude that BSA is surface active and has a dynamic process through which it adsorbs to the surface that is relevant to proteins in the ocean adsorbing to the surface under variable conditions of fatty acid films and variable temperatures, and that ocean relevant concentrations of sodium cations facilitate and enhance the surface adsorption of BSA.

The results presented provide a more nuanced understanding of the effects that ocean conditions have on the SSML and interfacial structure. It is necessary to acknowledge that observations drawn from our results are dissimilar to the ocean because it is a non-equilibrium system.

Future work should aid in determining the effect that the ocean's dynamic nature has on the surface structure.

Acknowledgements

A.A.E. and H.C.A. acknowledge funding from the National Science Foundation through the Center for Aerosol Impacts on Chemistry of the Environment (CAICE) under Grant No. CHE-1801971. J.B.C. acknowledges funding support from the National Science Foundation through Grant No. CHE-2102313. S.M.E. acknowledges funding support from the Regional and Global Model Analysis (RGMA) component of the Earth and Environmental System Modeling (EESM) program, within the U.S. Department of Energy's Office of Science. It is a direct contribution to the HiLAT-RASM project.

References

- (1) Hardy, J. T. The Sea Surface Microlayer: Biology, Chemistry and Anthropogenic Enrichment. *Prog. Oceanogr.* **1982**, *11* (4), 307–328. [https://doi.org/10.1016/0079-6611\(82\)90001-5](https://doi.org/10.1016/0079-6611(82)90001-5).
- (2) Tanoue, E. Detection of Dissolved Protein Molecules in Oceanic Waters. *Mar. Chem.* **1995**, *51* (3), 239–252. [https://doi.org/10.1016/0304-4203\(95\)00061-5](https://doi.org/10.1016/0304-4203(95)00061-5).
- (3) Roy, S. Distributions of Phytoplankton Carbohydrate, Protein and Lipid in the World Oceans from Satellite Ocean Colour. *ISME J.* **2018**, *12* (6), 1457–1472. <https://doi.org/10.1038/s41396-018-0054-8>.
- (4) Mustaffa, N. I. H.; Badewien, T. H.; Ribas-Ribas, M.; Wurl, O. High-Resolution Observations on Enrichment Processes in the Sea-Surface Microlayer. *Sci. Rep.* **2018**, *8* (1), 1–12. <https://doi.org/10.1038/s41598-018-31465-8>.
- (5) Thornton, D. C. O.; Brooks, S. D.; Chen, J. Protein and Carbohydrate Exopolymer Particles in the Sea Surface Microlayer (SML). *Front. Mar. Sci.* **2016**, *3* (AUG), 1–14. <https://doi.org/10.3389/fmars.2016.00135>.
- (6) Engel, A.; Bange, H. W.; Cunliffe, M.; Burrows, S. M.; Friedrichs, G.; Galgani, L.; Herrmann, H.; Hertkorn, N.; Johnson, M.; Liss, P. S.; Quinn, P. K.; Schartau, M.; Soloviev, A.; Stolle, C.; Upstill-Goddard, R. C.; van Pinxteren, M.; Zäncker, B. The Ocean's Vital Skin: Toward an Integrated Understanding of the Sea Surface Microlayer. *Front. Mar. Sci.* **2017**, *4* (MAY), 1–14. <https://doi.org/10.3389/fmars.2017.00165>.
- (7) Schiffer, J. M.; Luo, M.; Dommer, A. C.; Thoron, G.; Pendergraft, M.; Santander, M. V.; Lucero, D.; Pecora De Barros, E.; Prather, K. A.; Grassian, V. H.; Amaro, R. E. Impacts of Lipase Enzyme on the Surface Properties of Marine Aerosols. *J. Phys. Chem. Lett.* **2018**, *9* (14), 3839–3849. <https://doi.org/10.1021/acs.jpclett.8b01363>.
- (8) Luo, M.; Dommer, A. C.; Schiffer, J. M.; Rez, D. J.; Mitchell, A. R.; Amaro, R. E.; Grassian, V. H. Surfactant Charge Modulates Structure and Stability of Lipase-Embedded Monolayers at Marine-Relevant Aerosol Surfaces. *Langmuir* **2019**, *35* (27), 9050–9060. <https://doi.org/10.1021/acs.langmuir.9b00689>.

(9) Wilson, T. W.; Ladino, L. A.; Alpert, P. A.; Breckels, M. N.; Brooks, I. M.; Browse, J.; Burrows, S. M.; Carslaw, K. S.; Huffman, J. A.; Judd, C.; Kilthau, W. P.; Mason, R. H.; McFiggans, G.; Miller, L. A.; Najera, J. J.; Polishchuk, E.; Rae, S.; Schiller, C. L.; Si, M.; Temprado, J. V.; Whale, T. F.; Wong, J. P. S.; Wurl, O.; Yakobi-Hancock, J. D.; Abbatt, J. P. D.; Aller, J. Y.; Bertram, A. K.; Knopf, D. A.; Murray, B. J. A Marine Biogenic Source of Atmospheric Ice-Nucleating Particles. *Nature* **2015**, *525* (7568), 234–238. <https://doi.org/10.1038/nature14986>.

(10) Steinke, I.; Demott, P. J.; Deane, G. B.; Hill, T. C. J.; Maltrud, M.; Raman, A.; Burrows, S. M. A Numerical Framework for Simulating the Atmospheric Variability of Supermicron Marine Biogenic Ice Nucleating Particles. *Atmospheric Chem. Phys.* **2022**, *22* (2), 847–859. <https://doi.org/10.5194/acp-22-847-2022>.

(11) Orellana, M. V.; Matrai, P. A.; Leck, C.; Rauschenberg, C. D.; Lee, A. M.; Coz, E. Marine Microgels as a Source of Cloud Condensation Nuclei in the High Arctic. *Proc. Natl. Acad. Sci. U. S. A.* **2011**, *108* (33), 13612–13617. <https://doi.org/10.1073/pnas.1102457108>.

(12) Leck, C.; Bigg, E. K. Biogenic Particles in the Surface Microlayer and Overlaying Atmosphere in the Central Arctic Ocean during Summer. *Tellus B Chem. Phys. Meteorol.* **2005**, *57* (4), 305–316. <https://doi.org/10.3402/tellusb.v57i4.16546>.

(13) Schiffer, J. M.; Mael, L. E.; Prather, K. A.; Amaro, R. E.; Grassian, V. H. Sea Spray Aerosol: Where Marine Biology Meets Atmospheric Chemistry. *ACS Cent. Sci.* **2018**, *4* (12), 1617–1623. <https://doi.org/10.1021/acscentsci.8b00674>.

(14) Quinn, P. K.; Collins, D. B.; Grassian, V. H.; Prather, K. A.; Bates, T. S. Chemistry and Related Properties of Freshly Emitted Sea Spray Aerosol. *Chem. Rev.* **2015**, *115* (10), 4383–4399. <https://doi.org/10.1021/cr500713g>.

(15) Ault, A. P.; Moffet, R. C.; Baltrusaitis, J.; Collins, D. B.; Ruppel, M. J.; Cuadra-Rodriguez, L. A.; Zhao, D.; Guasco, T. L.; Ebbin, C. J.; Geiger, F. M.; Bertram, T. H.; Prather, K. A.; Grassian, V. H. Size-Dependent Changes in Sea Spray Aerosol Composition and Properties with Different Seawater Conditions. *Environ. Sci. Technol.* **2013**, *47* (11), 5603–5612. <https://doi.org/10.1021/es400416g>.

(16) Collins, D. B.; Ault, A. P.; Moffet, R. C.; Ruppel, M. J.; Cuadra-Rodriguez, L. A.; Guasco, T. L.; Corrigan, C. E.; Pedler, B. E.; Azam, F.; Aluwihare, L. I.; Bertram, T. H.; Roberts, G. C.; Grassian, V. H.; Prather, K. A. Impact of Marine Biogeochemistry on the Chemical Mixing State and Cloud Forming Ability of Nascent Sea Spray Aerosol. *J. Geophys. Res. Atmospheres* **2013**, *118* (15), 8553–8565. <https://doi.org/10.1002/jgrd.50598>.

(17) Wiesenburg, D. A.; Little, B. J. Synopsis of the Chemical/Physical Properties of Seawater. *Ocean Phys. Eng.* **1987**, *12* (3–4), 127–165.

(18) Li, Y.; Shrestha, M.; Luo, M.; Sit, I.; Song, M.; Grassian, V. H.; Xiong, W. Salting up of Proteins at the Air/Water Interface. *Langmuir* **2019**, *35* (43), 13815–13820. <https://doi.org/10.1021/acs.langmuir.9b01901>.

(19) Neurath, H.; Bull, H. B. The Surface Activity of Proteins. *Chem. Rev.* **1938**, *23* (3), 391–435. <https://doi.org/10.1021/cr60076a001>.

(20) Elliott, S.; Burrows, S.; Cameron-Smith, P.; Hoffman, F.; Hunke, E.; Jeffery, N.; Liu, Y.; Maltrud, M.; Menzo, Z.; Ogunro, O.; Van Roekel, L.; Wang, S.; Brunke, M.; Jin, M.; Letscher, R.; Meskhidze, N.; Russell, L.; Simpson, I.; Stokes, D.; Wingenter, O. Does Marine Surface Tension Have Global Biogeography? Addition for the OCEANFILMS Package. *Atmosphere* **2018**, *9* (6). <https://doi.org/10.3390/atmos9060216>.

(21) Ogunro, O. O.; Burrows, S. M.; Elliott, S.; Frossard, A. A.; Hoffman, F.; Letscher, R. T.; Moore, J. K.; Russell, L. M.; Wang, S.; Wingenter, O. W. Global Distribution and Surface Activity of Macromolecules in Offline Simulations of Marine Organic Chemistry. *Biogeochemistry* **2015**, *126* (1–2), 25–56. <https://doi.org/10.1007/s10533-015-0136-x>.

(22) Elliott, S.; Menzo, Z.; Jayasinghe, A.; Allen, H. C.; Ogunro, O.; Gibson, G.; Hoffman, F.; Wingenter, O. Biogeochemical Equation of State for the Sea-Air Interface. *Atmosphere* **2019**, *10* (5), 1–17. <https://doi.org/10.3390/atmos10050230>.

(23) McCoy, D. T.; Burrows, S. M.; Wood, R.; Grosvenor, D. P.; Elliott, S. M.; Ma, P. L.; Rasch, P. J.; Hartmann, D. L. Natural Aerosols Explain Seasonal and Spatial Patterns of Southern Ocean Cloud Albedo. *Sci. Adv.* **2015**, *1* (6). <https://doi.org/10.1126/sciadv.1500157>.

(24) Burrows, S. M.; Easter, R.; Liu, X.; Ma, P.-L.; Wang, H.; Elliott, S. M.; Singh, B.; Zhang, K.; Rasch, P. J. OCEANFILMS Sea-Spray Organic Aerosol Emissions – Part 1: Implementation and Impacts on Clouds. *Atmospheric Chem. Phys. Discuss.* **2018**, No. May, 1–27. <https://doi.org/10.5194/acp-2018-70>.

(25) Wierenga, P. A.; Egmond, M. R.; Voragen, A. G. J.; de Jongh, H. H. J. The Adsorption and Unfolding Kinetics Determines the Folding State of Proteins at the Air-Water Interface and Thereby the Equation of State. *J. Colloid Interface Sci.* **2006**, *299* (2), 850–857. <https://doi.org/10.1016/j.jcis.2006.03.016>.

(26) Xiao, Y.; Konermann, L. Protein Structural Dynamics at the Gas/Water Interface Examined by Hydrogen Exchange Mass Spectrometry. *Protein Sci.* **2015**, *24* (8), 1247–1256. <https://doi.org/10.1002/pro.2680>.

(27) Farber, P. J.; Mittermaier, A. Side Chain Burial and Hydrophobic Core Packing in Protein Folding Transition States. *Protein Sci.* **2008**, *17* (4), 644–651. <https://doi.org/10.1110/ps.073105408>.

(28) Argos, P.; Rossmann, M. G.; Grau, U. M.; Zuber, H.; Frank, G.; Tratschin, J. D. Thermal Stability and Protein Structure. *Biochemistry* **1979**, *18* (25), 5698–5703. <https://doi.org/10.1021/bi00592a028>.

(29) Abraham, J. P.; Baringer, M.; Bindoff, N. L.; Boyer, T.; Cheng, L. J.; Church, J. A.; Conroy, J. L.; Domingues, C. M.; Fasullo, J. T.; Gilson, J.; Goni, G.; Good, S. A.; Gorman, J. M.; Gouretski, V.; Ishii, M.; Johnson, G. C.; Kizu, S.; Lyman, J. M.; Macdonald, A. M.; Minkowycz, W. J.; Moffitt, S. E.; Palmer, M. D.; Piola, A. R.; Reseghetti, F.; Schuckmann, K.; Trenberth, K. E.; Velicogna, I.; Willis, J. K. A Review of Global Ocean Temperature Observations: Implications for Ocean Heat Content Estimates and Climate Change. *Rev. Geophys.* **2013**, *51* (3), 450–483. <https://doi.org/10.1002/rog.20022>.

(30) Morisset, J. D.; Pownall, H. J.; Gotto, A. M. Bovine Serum Albumin. Study of the Fatty Acid and Steroid Binding Sites Using Spin Labeled Lipids. *J. Biol. Chem.* **1975**, *250* (7), 2487–2494. [https://doi.org/10.1016/s0021-9258\(19\)41627-x](https://doi.org/10.1016/s0021-9258(19)41627-x).

(31) Gew, L. T.; Misran, M. Albumin-Fatty Acid Interactions at Monolayer Interface. *Nanoscale Res. Lett.* **2014**, *9* (1), 1–6. <https://doi.org/10.1186/1556-276X-9-218>.

(32) Meinders, M. B. J.; Van den Bosch, G. G. M.; De Jongh, H. H. J. Adsorption Properties of Proteins at and near the Air/Water Interface from IRRAS Spectra of Protein Solutions. *Eur. Biophys. J.* **2001**, *30* (4), 256–267. <https://doi.org/10.1007/s002490000124>.

(33) Martin, A. H.; Meinders, M. B. J.; Bos, M. A.; Stuart, M. A. C. Adsorption Properties and Conformational Aspects of Proteins at the Air-Water Interface Measured by Infra-Red Reflection Absorption Spectrometry. **2007**, 226–233. <https://doi.org/10.1039/9781847550835-00226>.

(34) Kudryashova, E. V.; Meinders, M. B. J.; Visser, A. J. W. G.; Van Hoek, A.; De Jongh, H. H. J. Structure and Dynamics of Egg White Ovalbumin Adsorbed at the Air/Water Interface. *Eur. Biophys. J.* **2003**, *32* (6), 553–562. <https://doi.org/10.1007/s00249-003-0301-3>.

(35) De Jongh, H. H. J.; Kosters, H. A.; Kudryashova, E.; Meinders, M. B. J.; Trofimova, D.; Wierenga, P. A. Protein Adsorption at Air-Water Interfaces: A Combination of Details. *Biopolymers* **2004**, *74* (1–2), 131–135. <https://doi.org/10.1002/bip.20036>.

(36) Meinders, M. B. J.; De Jongh, H. H. J. Limited Conformational Change of β -Lactoglobulin When Adsorbed at the Air-Water Interface. *Biopolym. - Biospectroscopy Sect.* **2002**, *67* (4–5), 319–322. <https://doi.org/10.1002/bip.10115>.

(37) Langmuir, I.; Waugh, D. F. The Adsorption of Proteins at Oil-Water Interfaces and Artificial Protein-Lipid Membranes the Adsorption of Proteins at Oil-Water Interfaces and Artificial Protein-Lipid Membranes. *J. Gen. Physiol.* **1938**, *745*–755. <https://doi.org/10.1085/jgp.21.6.745>.

(38) Jarvis, N. L.; Garrett, W. D.; Scheiman, M. A.; Timmons, C. O. Surface Chemical Characterization of Surface-Active Material in Seawater. *Limnol. Oceanogr.* **1967**, *12* (1), 88–96. <https://doi.org/10.4319/lo.1967.12.1.0088>.

(39) Noskov, B. A.; Mikhailovskaya, A. A.; Lin, S.-Y.; Loglio, G.; Miller, R. Bovine Serum Albumin Unfolding at the Air/Water Interface as Studied by Dilational Surface Rheology. *Langmuir* **2010**, *26* (22), 17225–17231. <https://doi.org/10.1021/la103360h>.

(40) Yuan, G.; Kienzle, P. A.; Satija, S. K. Salting Up and Salting Down of Bovine Serum Albumin Layers at the Air–Water Interface. *Langmuir* **2020**, *36* (50), 15240–15246. <https://doi.org/10.1021/acs.langmuir.0c02457>.

(41) Ulaganathan, V.; Retzlaff, I.; Won, J. Y.; Gochev, G.; Gunes, D. Z.; Gehin-Delval, C.; Leser, M.; Noskov, B. A.; Miller, R. β -Lactoglobulin Adsorption Layers at the Water/Air Surface: 2. Dilational Rheology: Effect of PH and Ionic Strength. *Colloids Surf. Physicochem. Eng. Asp.* **2017**, *521*, 167–176. <https://doi.org/10.1016/j.colsurfa.2016.08.064>.

(42) Cheng, Y. C.; Bianco, C. L.; Sandler, S. I.; Lenhoff, A. M. Salting-out of Lysozyme and Ovalbumin from Mixtures: Predicting Precipitation Performance from Protein-Protein Interactions. *Ind. Eng. Chem. Res.* **2008**, *47* (15), 5203–5213. <https://doi.org/10.1021/ie071462p>.

(43) Kang, B.; Tang, H.; Zhao, Z.; Song, S. Hofmeister Series: Insights of Ion Specificity from Amphiphilic Assembly and Interface Property. *ACS Omega* **2020**, *5* (12), 6229–6239. <https://doi.org/10.1021/acsomega.0c00237>.

(44) Zhou, H. X. Interactions of Macromolecules with Salt Ions: An Electrostatic Theory for the Hofmeister Effect. *Proteins Struct. Funct. Genet.* **2005**, *61* (1), 69–78. <https://doi.org/10.1002/prot.20500>.

(45) Grooms, A. J.; Neal, J. F.; Ng, K. C.; Zhao, W.; Flood, A. H.; Allen, H. C. Thermodynamic Signatures of the Origin of *Anti*-Hofmeister Selectivity for Phosphate at Aqueous Interfaces. *J. Phys. Chem. A* **2020**, *124* (27), 5621–5630. <https://doi.org/10.1021/acs.jpca.0c02515>.

(46) Hyde, A. M.; Zultanski, S. L.; Waldman, J. H.; Zhong, Y.-L.; Shevlin, M.; Peng, F. General Principles and Strategies for Salting-Out Informed by the Hofmeister Series. *Org. Process Res. Dev.* **2017**, *21* (9), 1355–1370. <https://doi.org/10.1021/acs.oprd.7b00197>.

(47) Zhang, Y.; Cremer, P. S. Interactions between Macromolecules and Ions: The Hofmeister Series. *Curr. Opin. Chem. Biol.* **2006**, *10* (6), 658–663. <https://doi.org/10.1016/j.cbpa.2006.09.020>.

(48) Noskov, B.; Mikhailovskaya, A. Adsorption Kinetics of Globular Proteins and Protein/Surfactant Complexes at the Liquid–Gas Interface. *Soft Matter* **2013**, *9* (39), 9392. <https://doi.org/10.1039/c3sm51357b>.

(49) Pedraz, P.; Montes, F. J.; Cerro, R. L.; Díaz, M. E. Characterization of Langmuir Biofilms Built by the Biospecific Interaction of Arachidic Acid with Bovine Serum Albumin. *Thin Solid Films* **2012**, *525*, 121–131. <https://doi.org/10.1016/j.tsf.2012.10.055>.

(50) Bian, H.; Feng, R.; Xu, Y.; Guo, Y.; Wang, H. Increased Interfacial Thickness of the NaF, NaCl and NaBr Salt Aqueous Solutions Probed with Non-Resonant Surface Second Harmonic

Generation (SHG). *Phys. Chem. Chem. Phys.* **2008**, *10* (32), 4920. <https://doi.org/10.1039/b806362a>.

(51) Abrosimova, K. V.; Shulenina, O. V.; Paston, S. V. FTIR Study of Secondary Structure of Bovine Serum Albumin and Ovalbumin. *J. Phys. Conf. Ser.* **2016**, *769* (1). <https://doi.org/10.1088/1742-6596/769/1/012016>.

(52) Grdadolnik, J.; Maréchal, Y. Bovine Serum Albumin Observed by Infrared Spectrometry. I. Methodology, Structural Investigation, and Water Uptake. *Biopolym. - Biospectroscopy Sect.* **2001**, *62* (1), 40–53. [https://doi.org/10.1002/1097-0282\(2001\)62:1<40::AID-BIP60>3.0.CO;2-C](https://doi.org/10.1002/1097-0282(2001)62:1<40::AID-BIP60>3.0.CO;2-C).

(53) Furlan, P. Y.; Scott, S. A.; Peaslee, M. H. FTIR-ATR Study of PH Effects on Egg Albumin Secondary Structure. *Spectrosc. Lett.* **2007**, *40* (3), 475–482. <https://doi.org/10.1080/00387010701295950>.

(54) Rabe, M.; Kerth, A.; Blume, A.; Garidel, P. Albumin Displacement at the Air–Water Interface by Tween (Polysorbate) Surfactants. *Eur. Biophys. J.* **2020**, *49* (7), 533–547. <https://doi.org/10.1007/s00249-020-01459-4>.

(55) Cheng, S.; Li, S.; Tsона, N. T.; George, C.; Du, L. Insights into the Headgroup and Chain Length Dependence of Surface Characteristics of Organic-Coated Sea Spray Aerosols. *ACS Earth Space Chem.* **2019**, *3* (4), 571–580. <https://doi.org/10.1021/acsearthspacechem.8b00212>.

(56) Wellen Rudd, B. A.; Vidalis, A. S.; Allen, H. C. Thermodynamic: Versus Non-Equilibrium Stability of Palmitic Acid Monolayers in Calcium-Enriched Sea Spray Aerosol Proxy Systems. *Phys. Chem. Chem. Phys.* **2018**, *20* (24), 16320–16332. <https://doi.org/10.1039/c8cp01188e>.

(57) Vazquez de Vasquez, M. G.; Rogers, M. M.; Carter-Fenk, K. A.; Allen, H. C. Discerning Poly- and Monosaccharide Enrichment Mechanisms: Alginate and Glucuronate Adsorption to a Stearic Acid Sea Surface Microlayer. *ACS Earth Space Chem.* **2022**. <https://doi.org/10.1021/acsearthspacechem.2c00066>.

(58) Vazquez De Vasquez, M. G.; Carter-Fenk, K. A.; McCaslin, L. M.; Beasley, E. E.; Clark, J. B.; Allen, H. C. Hydration and Hydrogen Bond Order of Octadecanoic Acid and Octadecanol Films on Water at 21 and 1°C. *J. Phys. Chem. A* **2021**, *125* (46), 10065–10078. <https://doi.org/10.1021/acs.jpca.1c06101>.

(59) Carter-Fenk, K. A.; Dommer, A. C.; Fiamingo, M. E.; Kim, J.; Amaro, R. E.; Allen, H. C. Calcium Bridging Drives Polysaccharide Co-Adsorption to a Proxy Sea Surface Microlayer. *Phys. Chem. Chem. Phys.* **2021**, *23* (30), 16401–16416. <https://doi.org/10.1039/d1cp01407b>.

(60) Kudryashova, E. V. Reversible Self-Association of Ovalbumin at Air-Water Interfaces and the Consequences for the Exerted Surface Pressure. *Protein Sci.* **2005**, *14* (2), 483–493. <https://doi.org/10.1110/ps.04771605>.

(61) Lad, M. D.; Birembaut, F.; Matthew, J. M.; Frazier, R. A.; Green, R. J. The Adsorbed Conformation of Globular Proteins at the Air/Water Interface. *Phys. Chem. Chem. Phys.* **2006**, *8* (18), 2179–2186. <https://doi.org/10.1039/b515934b>.

(62) Lad, M. D.; Birembaut, F.; Frazier, R. A.; Green, R. J. Protein – Lipid Interactions at the Air / Water Interface. *PCCP* **2005**, *7*, 3478–3485.

For TOC use only

Bovine Serum Albumin (BSA) Surface Adsorption

H_2O @ 10 °C \approx H_2O @ 20 °C ASW @ 10 °C < ASW @ 20 °C

